

## Scattering Parameter Measurements of the Long Wavelength Array Antenna and Front End Electronics

CHRISTOPHER DiLULLO <sup>1</sup>, WHITHAM D. REEVE <sup>2</sup>, BRIAN C. HICKS <sup>3</sup>, AND JAYCE DOWELL <sup>4</sup>

<sup>1</sup>*NASA Goddard Space Flight Center  
Observational Cosmology Laboratory, Code 665  
8800 Greenbelt Rd.  
Greenbelt, MD 20771*

<sup>2</sup>*Reeve Engineers  
2211 Kissee Ct.  
Anchorage, AK 99517*

<sup>3</sup>*Naval Research Laboratory  
Rapid Prototyping and Engineering Section, Code 7212  
4555 Overlook Ave. SW  
Washington, DC 20032*

<sup>4</sup>*University of New Mexico  
210 Yale Blvd. NE  
Albuquerque, NM 87131*

### ABSTRACT

We present recent 2–port vector network analyzer (VNA) measurements of the complete set of scattering parameters for the antenna used within the Long Wavelength Array (LWA) and the associated front end electronics (FEEs). Full scattering parameter measurements of the antenna yield not only the reflection coefficient for each polarization, S<sub>11</sub> and S<sub>22</sub>, but also the coupling between polarizations, S<sub>12</sub> and S<sub>21</sub>. These had been previously modeled using simulations, but direct measurements had not been obtained until now. The measurements are used to derive a frequency dependent impedance mismatch factor (IMF) which represents the fraction of power that is passed through the antenna–FEE interface and not reflected due to a mismatch between the impedance of the antenna and the impedance of the FEE. We also present results from a two antenna experiment where each antenna is hooked up to a separate port on the VNA. This allows for cross–antenna coupling to be measured for all four possible polarization combinations. Finally, we apply the newly measured IMF and FEE forward gain corrections to LWA data to investigate how well they remove instrumental effects.

### 1. INTRODUCTION

In a linear electrical system, the scattering parameters describe how incident power is either reflected or transmitted at a boundary. In a 2–port measurement, four scattering parameters can be measured by sending a signal from Port 1 to Port 2 and from Port 2 to Port 1: S<sub>11</sub>, S<sub>21</sub>, S<sub>12</sub>, and S<sub>22</sub> which describe the reflected power in Port 1, the transmitted power from Port 1 to Port 2, the transmitted power from Port 2 back to Port 1, and the reflected power at Port 2, respectively. Measuring the S<sub>11</sub> and S<sub>22</sub> parameters is equivalent to measuring the mismatch in electrical impedance at the boundary.

A mismatch between the impedance of any antenna and the impedance of its associated electronics will cause some reflection of power. In a receiving system such as a radio telescope, this reflection of power corresponds to a loss of sensitivity that is frequency dependent. This frequency dependent loss of sensitivity is an issue for experiments which require absolute calibration of the telescope since this effect must be quantified in order to set the absolute zero calibration level. However, if the reflection coefficients can be directly measured using a Vector Network Analyzer

(VNA), then the relative efficiency of the system as a function of frequency, known as the impedance mismatch factor (IMF; Rudge et al. 1986), can be computed. The IMF can be applied as a correction to data to remove impedance mismatch effects and can be expressed as

$$IMF = \frac{(1 - |\Gamma_{ant}|^2)(1 - |\Gamma_{RX}|^2)}{|1 - \Gamma_{ant}\Gamma_{RX}|^2}, \quad (1)$$

where  $\Gamma_{ant}$  and  $\Gamma_{RX}$  are the reflection coefficients of the antenna and receiving electronics, respectively.

The Long Wavelength Array (LWA) is a low frequency radio telescope consisting of two stations in New Mexico, USA and a third station in California, USA. LWA1 (Taylor et al. 2012) is colocated with the Karl. J. Jansky Very Large Array (VLA) in Socorro, New Mexico, LWA-SV (Cranmer et al. 2017) is located on the Sevilleta National Wildlife Refuge in New Mexico, and LWA-OVRO is located at the Owens Valley Radio Observatory in California. The New Mexico stations are antenna arrays consisting of 256 elements with pseudo-random placement while LWA-OVRO is currently being upgraded to support 352 elements with a different array geometry. The LWA antenna (Hicks et al. 2012) consists of two perpendicular “blade” dipoles whose geometry was chosen to balance cost, stability, and RF performance. The LWA antenna has been deployed by numerous groups all over the world due to its low cost, robust stability, wideband RF performance, and ease of construction.

Hicks et al. (2012) simulated the impedance of the LWA antenna and converted this into an impedance matching efficiency (IME) given by

$$IME = 1 - |\Gamma_{ant}|^2, \quad (2)$$

which is simply Equation 1 under the assumption that  $\Gamma_{RX} = 0$ . However, it is unlikely that the FEEs have no reflection at all, i.e. the FEE is not perfectly matched to a reference impedance of  $50 \Omega$  that is constant in frequency. Thus, actual measurements of both the antenna and FEEs were required for a more accurate picture of the impedance mismatch properties of the system. The current LWA experiments requiring a better understanding of the impedance mismatch characteristics, are the LWA1 Low Frequency Sky Survey (LWA1 LFSS; Dowell et al. 2017) and the effort to detect the redshifted 21 cm signal from neutral hydrogen present during the formation of the first stars (DiLullo et al. 2020, 2021). The LWA1 LFSS is the major driver of the work presented here because an impedance mismatch correction is applied to the raw data at the first step of calibration. The resulting absolute temperature calibration of the survey is reliant on this correction and so any errors in the correction will follow through the entire calibration pipeline. It is therefore important to make actual measurements of the impedance mismatch factor so that the limitations of the model presented in Hicks et al. (2012) could be better understood and an improved correction could be applied to previous and future survey data.

This paper details work carried out in November of 2022 which made direct measurements of the LWA antenna scattering parameters at three locations in New Mexico and the scattering parameters of the LWA FEEs, which were measured in February of 2023. Custom Calibration Fixtures were designed in order to de-embed the FEE from the antenna measurements. Cross-antenna coupling measurements were also performed by connecting two nearby antennas to each port of the VNA. Mutual coupling between antennas will change their electromagnetic properties, such as impedance and gain pattern, in a way that is not easy to model due to the shear complexity of the problem and required computation time. This is a concern for both the LWA1 LFSS and the 21 cm cosmology experiment at LWA-SV, referenced above, since these projects use models of the antenna gain pattern to set their calibration. Attempts have been made to model the effects of mutual coupling for a LWA station using method of moments simulations (Ellingson 2011); however, actual measurements have been impossible until now. The paper is structured as follows: Section 2 details the custom calibration and test fixtures which were designed for this experiment, Section 3 details the single antenna measurements, the antenna-antenna coupling measurements, and presents the results from each, and Section 4 discusses the results and applies them as new corrections to LWA1 data to investigate how they capture instrumental effects compared to older corrections.

## 2. CUSTOM CALIBRATION AND TEST FIXTURES

Calibration of a VNA requires three calibration standards: Open, Short, and Load which correspond to infinite resistance, zero resistance, and  $50 \Omega$  resistance, respectively. These references are typically not difficult to fabricate for use at low frequencies; however, in the case of the LWA antenna it was slightly more difficult due to the  $180^\circ$  hybrid coupler which exists on the FEE boards. The hybrid coupler acts as a balun between the balanced dipole feedpoints

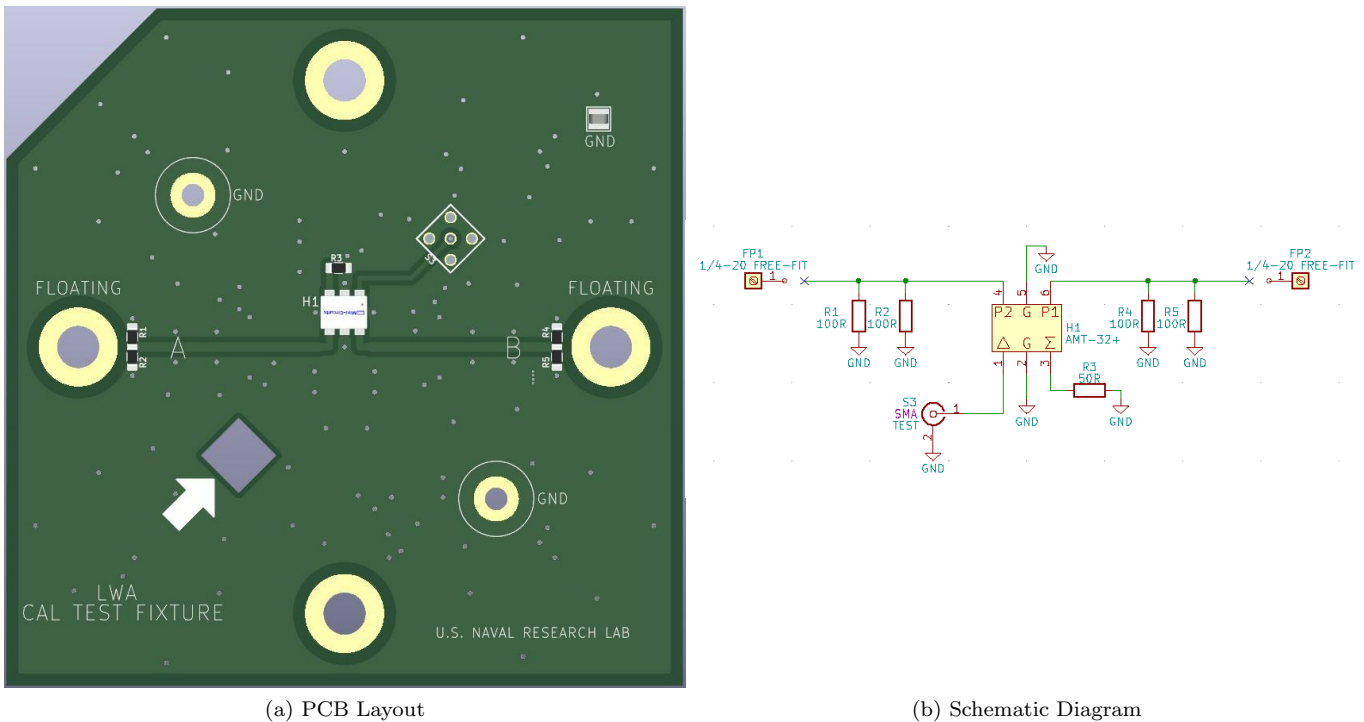
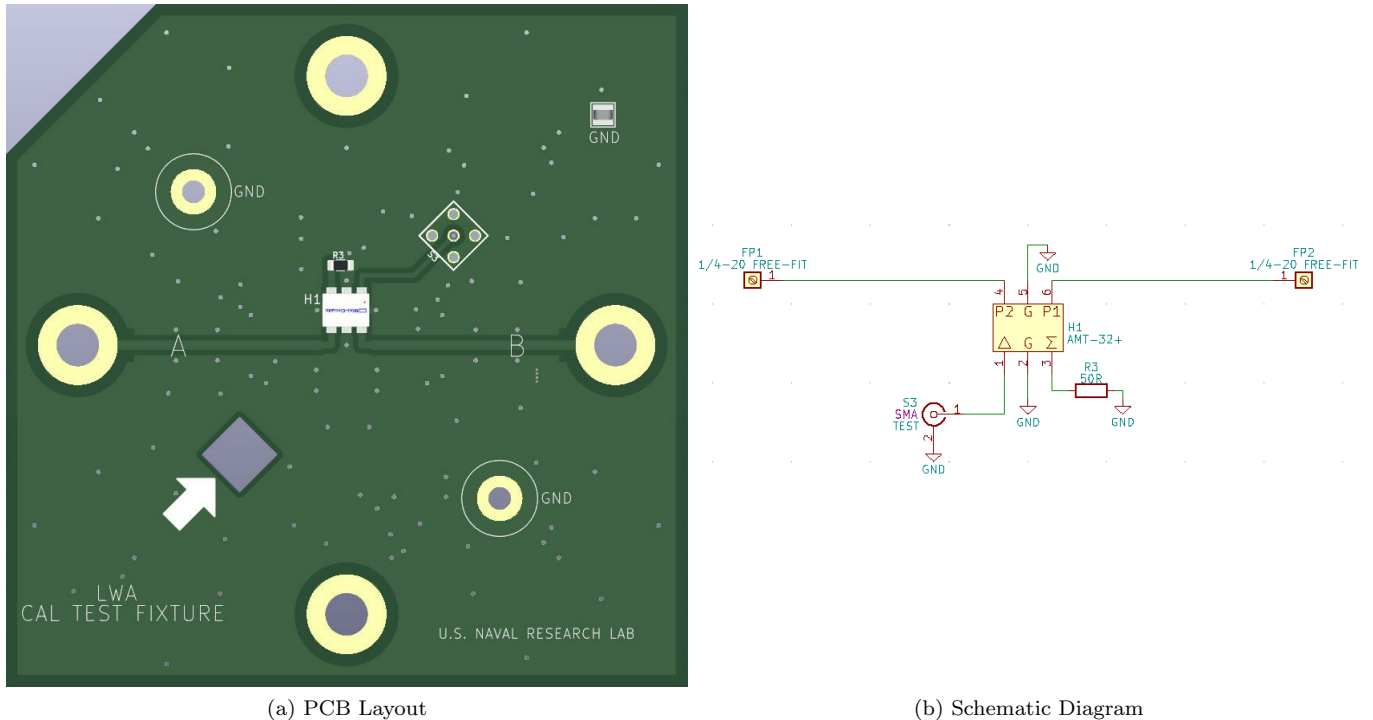


**Figure 1.** Calibration Fixtures. (a) CAD model showing the layout of a Calibration Fixture PCB with the  $180^\circ$  hybrid coupler shown at the center. The pads at the end of the traces by the circular feed point holes are for the different calibration resistors. The Open standard has no resistors, the Short standard has two  $0\ \Omega$  resistors in parallel, and the Load standard has two  $100\ \Omega$  resistors in parallel. The traces to the connector and hybrid coupler sum load also are visible. The PCB are made from FR4 glass epoxy material and their dimensions are 4.5 in x 4.5 in (114 mm x 114 mm). Each complete Calibration Fixture consists of two PCBs mounted back-to-back. (b) Schematic diagram showing the hybrid coupler at the center, connector, hybrid coupler sum load and the resistor pads at the end of the traces that run to the dipole feedpoints.

and unbalanced coaxial cables that carry the signal to the backend electronics. See [Hicks et al. \(2012\)](#) and associated references for more detailed information on the LWA FEE board design.

Custom VNA Calibration Fixtures were designed to include a TeleTech model HX62A hybrid coupler so that its effects could be de-embedded, thus moving the measurement reference plane from the VNA to the antenna feedpoints on the antenna hub. The single differential input from the antenna feedpoints into the HX62A hybrid coupler is treated as two single ended inputs which are referenced to ground. The impedance of each of these single inputs as well as the delta output port is  $50\ \Omega$ . The Calibration Fixtures use printed circuit boards (PCBs) with the same shape and dimensions as the FEE PCBs, but having traces only to pads near the dipole feedpoints where the calibration resistors are installed. The pads for the calibration resistors are symmetrical about the traces; thus, a Short is achieved by two parallel  $0\ \Omega$  resistors, a  $50\ \Omega$  Load is achieved by two parallel  $100\ \Omega$  resistors, and an Open is achieved by not populating the pads with any resistors. The traces from the hybrid coupler do not connect to the feedpoints. The Calibration Fixtures also include a coaxial connector and  $50\ \Omega$  load resistor for the hybrid coupler sum port. A CAD model and the associated schematic diagram of the Calibration Fixtures can be seen in [Figure 1](#). Commercial VNA calibration kits include a set of parameters that describe the delays and frequency-dependent coefficients for capacitance and inductance of the calibration standards. These parameters were set to zero for the custom calibration standards because the Open, Short, and Load were placed within a millimeter of the feedpoint reference plane, and capacitance and inductance effects at the low frequencies of interest are negligible.

Three Calibration Fixtures were fabricated. The three Calibration Fixtures each consist of a pancake of two identical PCBs, in the same manner as the FEE, which allows the Fixture to connect to both antenna polarizations. A Thru calibration fixture also was fabricated for complete 2-port calibration since both ports on the VNA are required for the single antenna and antenna mutual coupling measurements. The Thru Calibration Fixture consists of two Test Fixtures, described below, which are connected to each other at the balanced feedpoints and is classified as an Unknown Thru.



(a) PCB Layout

(b) Schematic Diagram

**Figure 2.** Test Fixture. (a) CAD model showing the layout of a Test Fixture PCB. The layout is identical to the Calibration Fixtures except there are no resistor pads and the traces from the hybrid coupler run directly to the feedpoints. (b) Schematic diagram.

In addition to the Calibration Fixtures, a set of Test Fixtures was fabricated to connect the VNA to the antenna-under-test for scattering parameter measurements after calibration. The test fixtures had the same dimensions and layout as the Calibration Fixtures and included the hybrid coupler; however, they did not include pads for the Open, Short, or Load resistors. Instead, the traces from the hybrid coupler on the Test Fixture connects to the dipole feedpoints as seen in Figure 2. Antenna mutual coupling measurements required a Test Fixture on each antenna, so two nominally identical sets of Test Fixtures were fabricated. See Section 3.2 for more details.

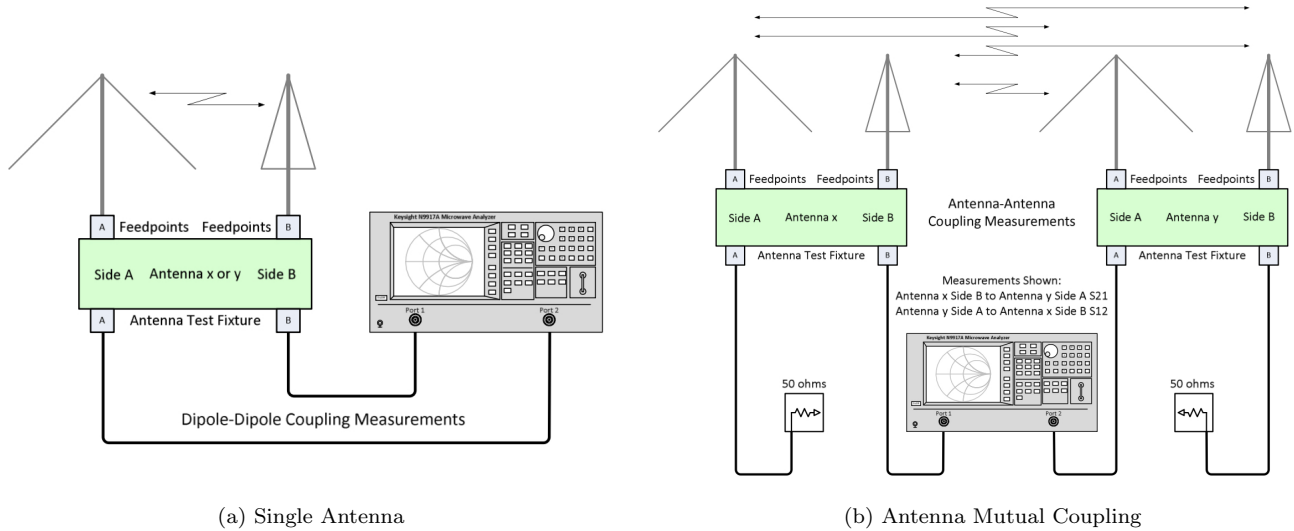
### 3. MEASUREMENTS AND RESULTS

*In situ* scattering parameter measurements were taken between November 10–11<sup>th</sup>, 2022 at both commissioned stations in New Mexico, LWA1 and LWA–SV, as well as an isolated antenna which was setup at a third site at the end of the northern arm of the VLA which will soon house another LWA station (LWA–NA). The measurements were divided into two types: single antenna, which measures the scattering parameters using a single antenna-under-test, and antenna mutual coupling, which uses two test fixtures and two adjacent antennas-under-test in order to measure the strength of mutual coupling between adjacent antennas in the array. The following sections discuss the setup and procedures for each of the measurement types. A Keysight Technologies N9917A FieldFox vector network analyzer was used for all antenna measurements. The measurements were carried out between 5 and 200 MHz with an IF bandwidth of 10 kHz and spectral resolution of 195 kHz. All measurement procedure documentation, data, and scripts used in the following analysis are freely available on [GitHub](https://github.com/lwa-project/Antenna_Impedance)<sup>1</sup>.

#### 3.1. Single Antenna Measurements

The single antenna measurements were setup using a single antenna-under-test where the two perpendicular polarizations are connected to the two ports on the VNA. See Figure 3 for an illustrative diagram of the setup. First, the VNA was calibrated using the Calibration Fixtures described in Section 2. A two port calibration of the VNA was carried out where each port was calibrated independently using the same calibration standards and two 11 m cables. The cables were laid as close as possible to existing antenna cables in order to best replicate how the antenna

<sup>1</sup> [https://github.com/lwa-project/Antenna\\_Impedance](https://github.com/lwa-project/Antenna_Impedance)



(a) Single Antenna

(b) Antenna Mutual Coupling

**Figure 3.** Example measurement setups for both types of measurements. The thin arrowed lines denote coupling paths that each type of measurement is sensitive to. (a) Single antenna measurements where polarization B of the antenna is connected to Port 1 and polarization A is connected to Port 2. (b) Antenna mutual coupling measurements where polarization B of antenna X is connected to Port 1 and polarization A of antenna Y is connected to Port 2. The inactive dipoles were terminated in 50 ohms via the test cables as shown. Measuring each polarization of each antenna was accomplished by simply reconnecting the cables at the Test Fixture to the desire polarization.

is usually setup. An Unknown Thru was used in the last calibration step to connect Port 1 to Port 2 once both ports were independently calibrated.

The Test Fixture described in Section 2 was then used to make the scattering parameter measurements. These measurements not only allow for reflection parameters to be measured for the independent dipole polarizations via measurements of  $S_{11}$  and  $S_{22}$ , it also allows for measurements of the cross-coupling between the individual dipole arms via measurements of  $S_{12}$  and  $S_{21}$ . We denote this coupling as “dipole-dipole coupling”, which should not be confused with mutual coupling between separate antennas, discussed in Section 3.2. Measurements were made at different antenna locations within the array to capture any location-dependent effects that might change the response of antennas deeply embedded within the array.

The results for LWA1 and LWA-SV are shown in Figure 4. We find that the two pairs:  $S_{11}$  and  $S_{22}$ ; and  $S_{21}$  and  $S_{12}$ , for each measured antenna, are generally reciprocal. This is encouraging to see despite the lack of symmetry in the antenna environments. Differences between the quality of each polarization arm or their environments, e.g. variances in construction or varying distances to nearby antennas, can result in variances between  $S_{11}$  and  $S_{22}$ , or  $S_{21}$  and  $S_{12}$ ; however, we only find variance on the order of the noise level of the measurements. It is also apparent from Figure 4 that the variances between scattering parameters across antennas is small, which again would not be generally expected due to variances in their respective environments within the array. This implies that it is a reasonable assumption that different antennas across the array have similar impedance characteristics.

We note a deep resonance around 125 MHz, but in the typical LWA observing band between 10–88 MHz the typical amplitudes of  $S_{11}$  and  $S_{22}$  are between -3 dB and -5 dB. However,  $S_{11}$  and  $S_{22}$  approach 0 dB, i.e. the antenna becomes almost entirely reflective, at frequencies  $\nu \lesssim 25$  MHz which implies the sensitivity of the array degrades at these frequencies. The presence of a ripple of unknown origin can be seen in the  $S_{11}$  and  $S_{22}$  measurements of order  $\sim 10$  MHz at both LWA1 and LWA-SV. Ripple-like structures can arise from many types of calibration errors that might be present during field measurements such as these. A few examples of such an errors would be drifts in cable performance due to temperature variations throughout the measurements and possible cable reflections due to a mismatch between the source impedance and cable impedance. However, we believe the former scenario to be unlikely as the VNA was calibrated immediately before the measurements were made at each antenna and the ambient temperature was relatively stable over the course of a single measurement. Cable reflections could possibly explain the ripple since the cables were 11 m long LMR-240 cables with a velocity ratio,  $v/c = 0.84$ . This could cause a ripple

with a characteristic scale of 11.4 MHz, which is close to the  $\sim 10$  MHz ripple seen; however, we again believe our calibration procedure would have captured an effect such as this.

We see a deep resonance in S11 for antenna 162 at LWA–SV centered around 38.5 MHz with an amplitude of -15 dB, but do not see such an extreme feature in the measurements of other antennas. We conclude this feature is anomalous since the other measurements agree that the amplitude of this dip is more on the order of -3.5 dB. The amplitudes of S12 and S21, which measure the amplitude of cross-coupling between antenna polarizations, are very small with averages of -46 dB. This means that we do not expect any appreciable amount of polarization leakage which can degrade the sensitivity of the antenna and the station as a whole.

The results for an isolated antenna are shown in Figure 5. This was a single antenna setup at the future LWA–NA site and therefore represents the most isolated measurement of a LWA antenna. The measurements at both LWA1 and LWA–SV suffer from some degree of antenna–antenna mutual coupling, but this was avoided at LWA–NA since no other antennas there have been constructed. We find good agreement between the measurements taken at LWA–NA and the other stations.

### 3.2. Antenna Mutual Coupling

The antenna mutual coupling measurements used two adjacent antennas in the array to measure how strongly one polarization of the first antenna couples to a polarization of the second. The setup can be seen in Figure 3. We denote the two antennas in the setup as Antenna X and Antenna Y and the two polarizations on each as A and B. Therefore, there are a total of 4 permutations that were measured in order to capture the full coupling. Whichever polarization that was not being tested on each antenna was connected to a  $50 \Omega$  termination to isolate that polarization so it will not affect the coupling results.

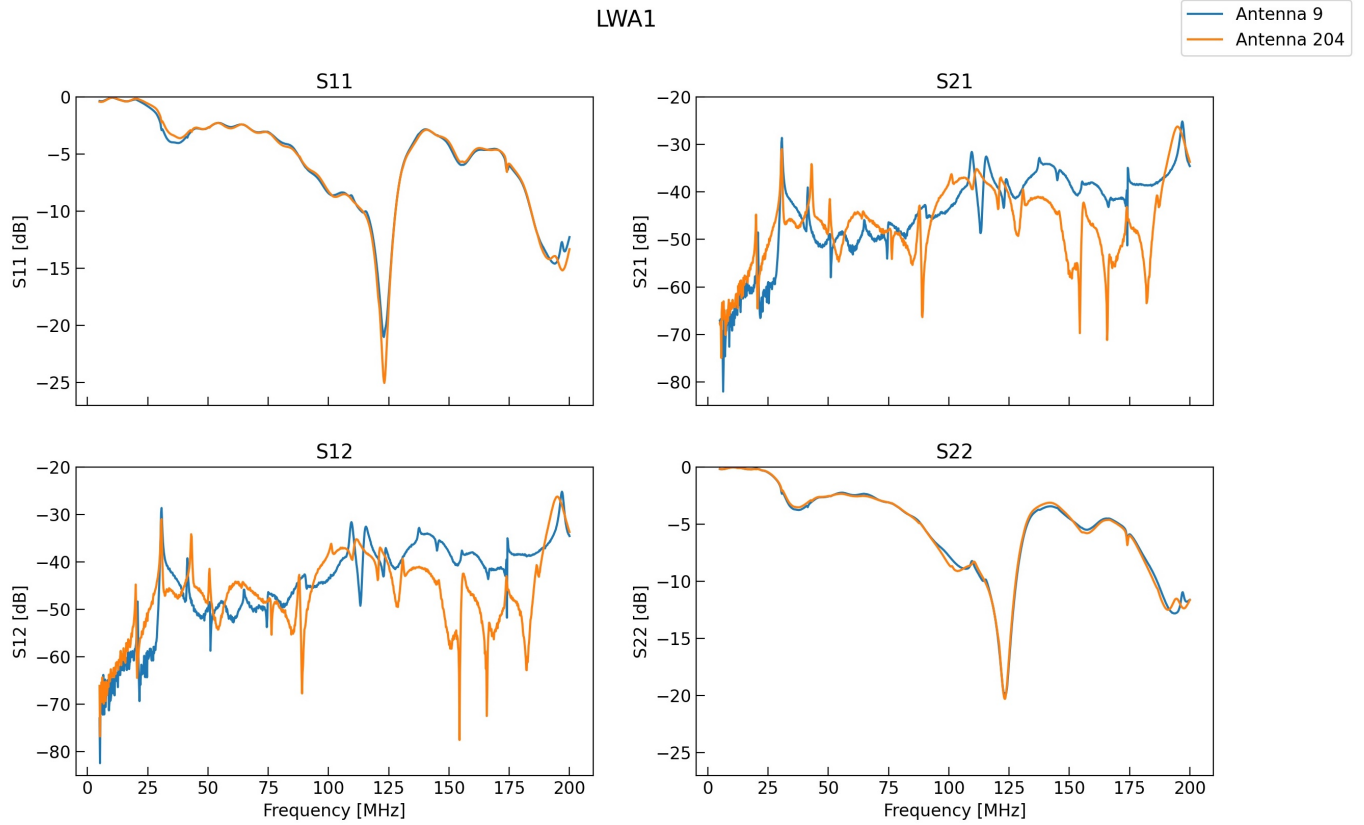
The two ports of the VNA were independently calibrated in the same manner as the single antenna measurements. The Thru calibration was achieved by using the Thru Calibration Fixture, see Section 2, to connect Port 1 to Port 2. The cables which were not terminated to  $50 \Omega$  were pulled through the individual antenna masts and connected to the Thru Calibration Fixture in the middle of the two antennas. Two Test Fixtures were used to essentially turn one antenna into a transmitter and the other into a receiver. The minimum spacing between two antennas in a LWA array is 5.0 m in order to reduce mutual coupling effects in real observations. We chose antennas 9 and 10 at LWA1, which are separated by a distance of 5.9 m, and antennas 90 and 92 at LWA–SV, which are separated by a distance of 5.2 m. The scattering parameters S12 and S21 measure the coupling strength between the two antennas for a given polarization combination and their measurements are totally reciprocal. Figures 6 and 7 show the locations of the measured antennas within the arrays and the measured values of S12 for each of the polarization combinations at LWA1 and LWA–SV, respectively.

These results are limited in their ability to capture the full effect of mutual coupling between antennas since it is dependent on all the antennas in the array and is highly nonlinear. The amplitude of mutual coupling will vary between antennas and is likely dependent on the location within the array; however, these measurements should yield a sense of the general amplitude of the coupling. We find that the mutual coupling between antennas is small with the largest observed coupling in the LWA observable frequency range of 3–88 MHz being on the order of -30 dB. These data could be useful in developing a statistical model describing how mutual coupling of this amplitude can perturb the synthesized station beam pattern, but that is left for future work.

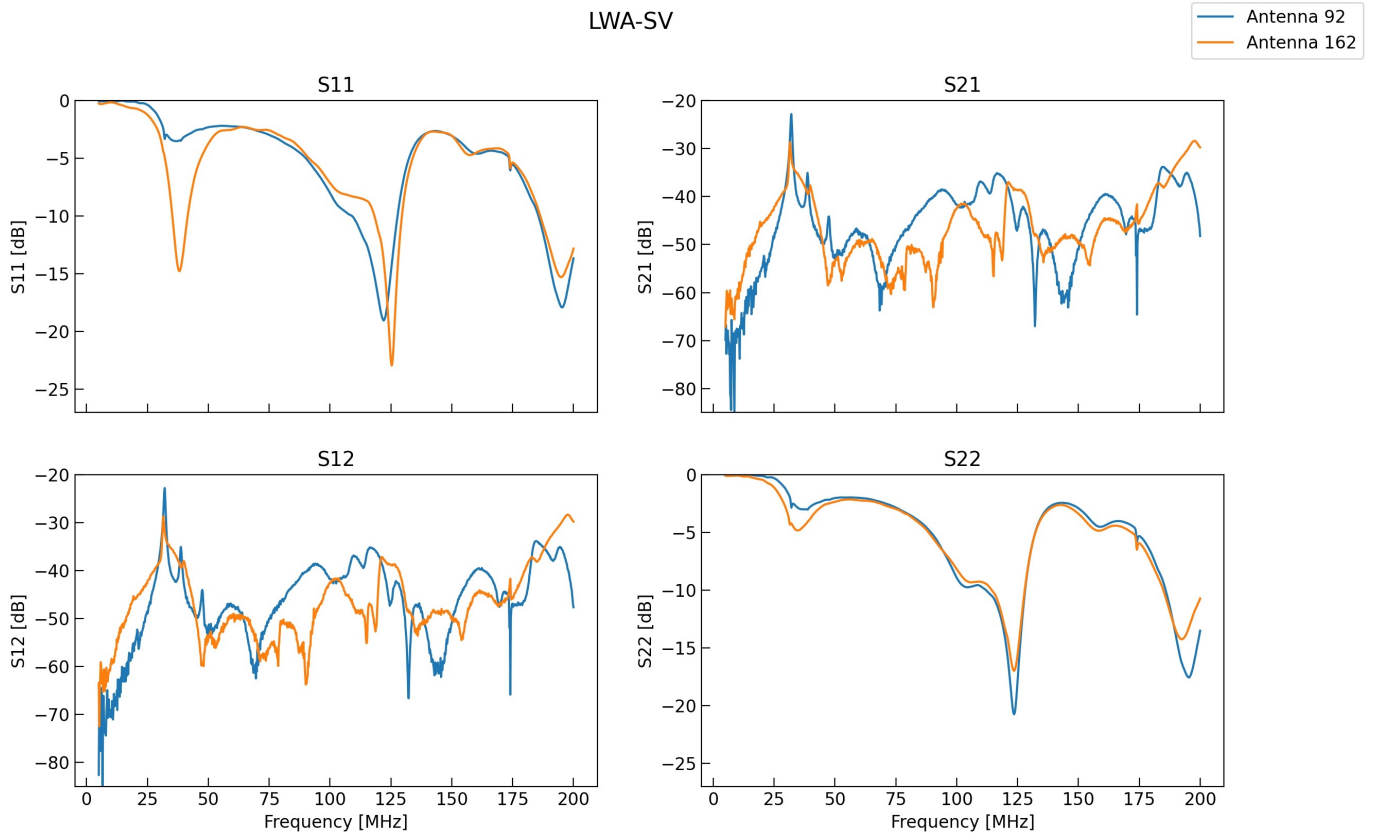
### 3.3. Impedance Mismatch Factor

The major goal of the work presented here was to use the scattering parameter measurements to calculate a new impedance mismatch factor, see Equation 1, that would better capture the impedance mismatch between the antenna and the FEEs than previous electromagnetic simulations of both could. Therefore, in order to properly compute the IMF, the scattering parameters for the FEE boards had to be measured also. There are currently two versions of the LWA FEE board: the version 1.8, which has been in use for the past few years, and the version 2.0, which is newly developed with many improvements over the version 1.8. A paper detailing the version 2.0 FEE is in development and the boards are just now becoming available, so the following work uses the version 1.8 FEE board.

The scattering parameter measurements of the FEE were carried out in a fashion similar to that of the antennas. A custom FEE Test Fixture box was fabricated that runs the signal from the VNA through a TeleTech HX62A hybrid coupler in reverse so the signal can be converted from the unbalanced coaxial cables on the VNA to a balanced signal which is injected into the FEE–under–test. It consists of two bays, an upper bay and a lower bay, with the FEE



(a) LWA1



(b) LWA-SV

**Figure 4.** Single antenna scattering parameter measurements at the two completed LWA stations in New Mexico. (a) LWA1 measurements where antenna 9 is deeply embedded within the array and antenna 204 is on the edge. (b) LWA-SV measurements where antenna 92 is deeply embedded within the array and antenna 162 is on the edge.

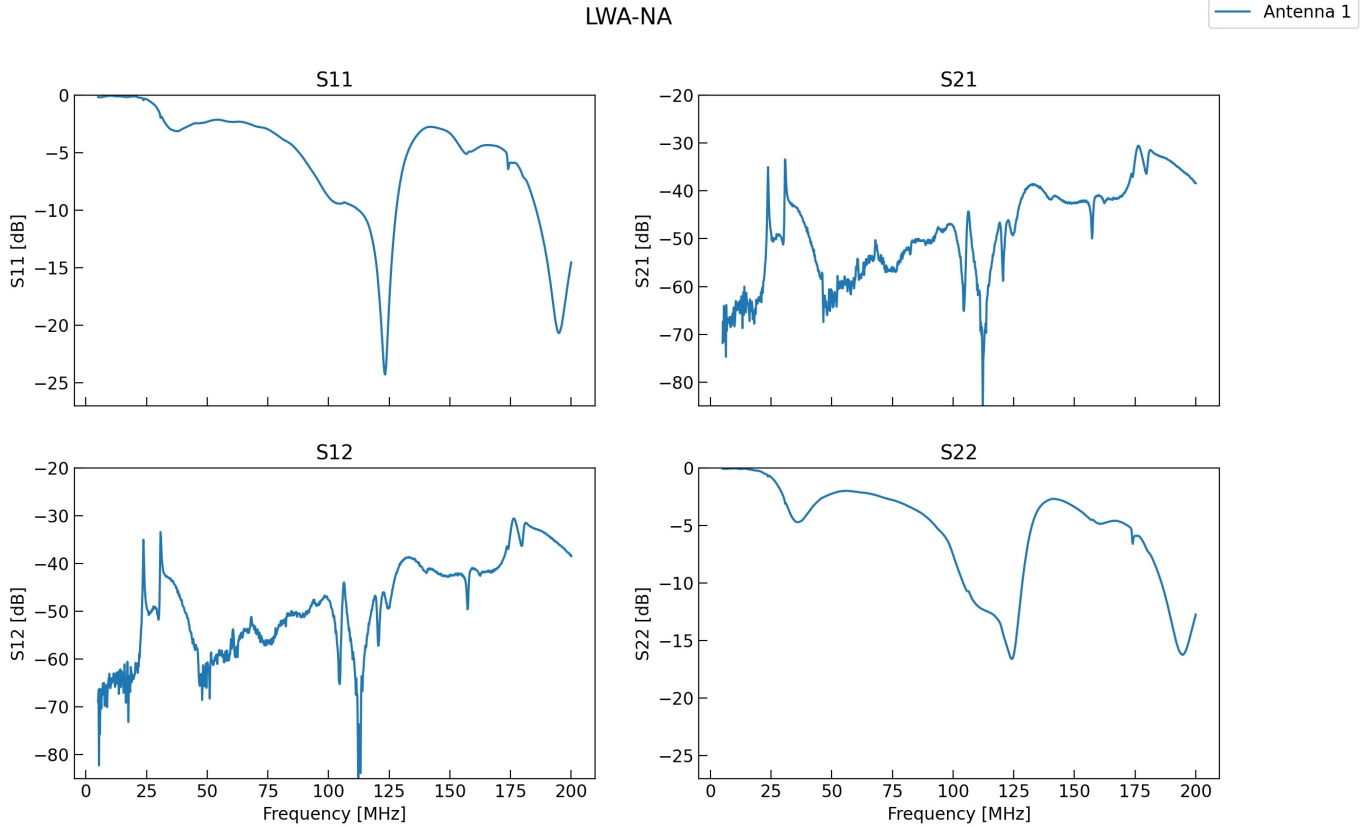


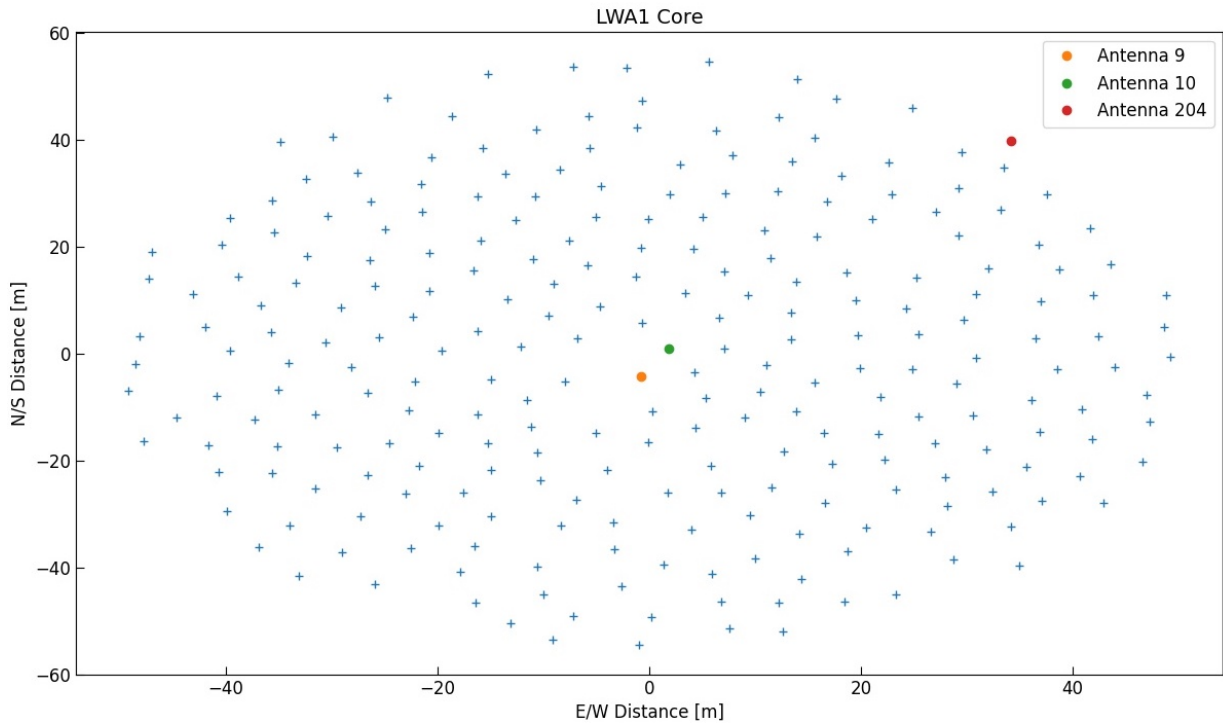
**Figure 5.** Scattering parameter measurements for a single antenna built at the future LWA-NA site. This is the most isolated measurement of a LWA antenna with regard to the presence of other antennas.

mounted in the upper bay on a Coupler PCB which has a hybrid coupler. The lower bay consists of a 15 Vdc power supply which powers the FEE through a bias tee. Labelled photos of the FEE Test Fixture and the upper and lower bays can be seen in Figure 8. This custom mount allows for measurements of a single polarization of the FEE board, but the cables can be easily switched to measure the second polarization. Two port measurements of the FEE board also allow for updated measurements of the FEE forward gain through measurement of the FEE’s S21 parameter. This is also used as a correction to the data in the LWA1 Low Frequency Sky Survey and is therefore also of great interest.

However, the presence of the hybrid coupler connecting the VNA to the FEE—under—test means that the reference plane of the VNA is no longer at the feedpoints of the FEE board, but rather it is where the coaxial cable connects to the hybrid coupler. Calibration of the VNA using the custom Calibration Fixtures described in Section 2 was carried out in order to de—embed the hybrid coupler. The calibration was achieved by connecting the VNA to proxy cables which account for the connections which are internal to the FEE Test Fixture box and then connecting the Short, Open, Load, and Thru Calibration Fixtures to Port 1 on the VNA. Port 2 was calibrated using standard SMA-F calibration standards. This 2—port calibration once again shifts the reference plane of Port 1 to the feedpoints of the FEE where the board mounts to the antenna and that of Port 2 to output of the FEE. A schematic view of the calibration and measurement procedures is shown in Figure 9.

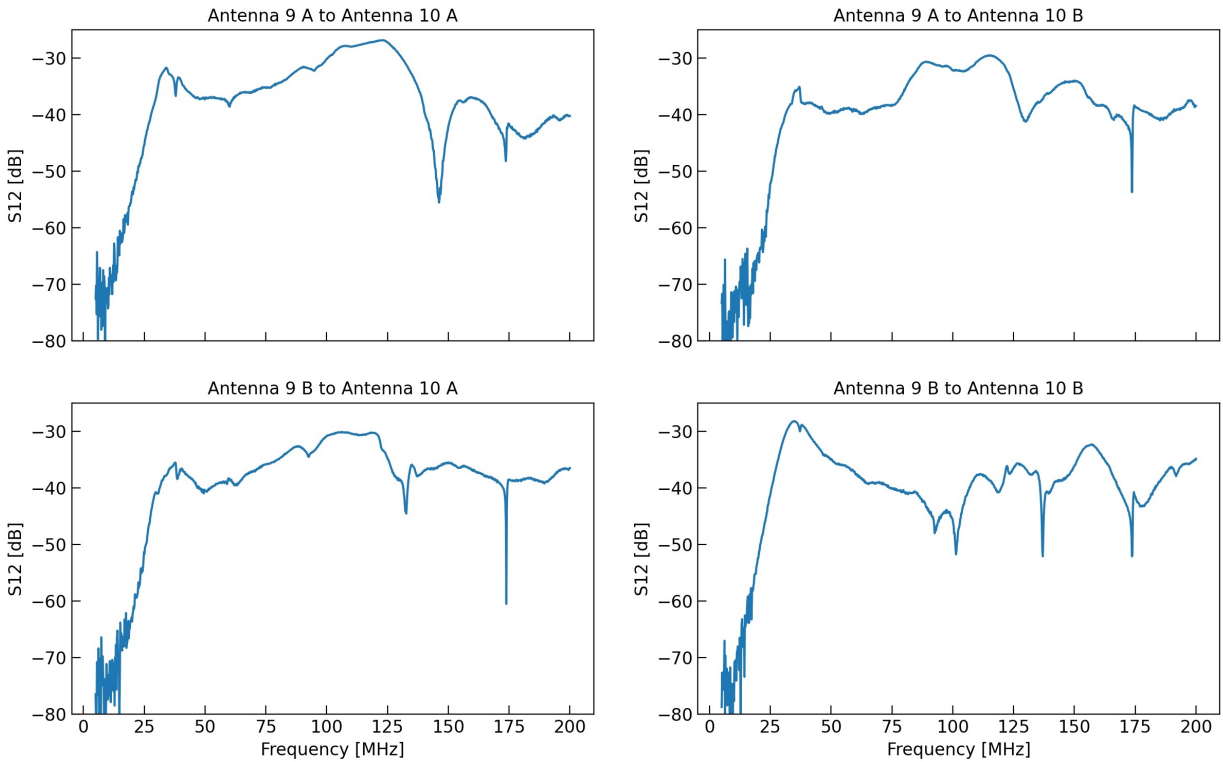
A set of 10 version 1.8 FEE boards was used in order to get better statistics compared to a single measurement. Slight variances in components, manufacturing, or repairs to the boards can result in changes to the scattering parameters, so it is better to compute the average scattering parameters from a set of FEEs. While 10 is not a very large sample, it allows for simple statistics like mean and standard deviation of the scattering parameters to be measured. The complete set of scattering parameters is shown in Figure 10. The S11 measurements were then used in combination with the single antenna measurements to compute the IMF via Equation 1. Antenna 162 at LWA-SV was omitted since it shows features in S11 which do not agree with the other measured antennas. This yields a total set of 30 IMF curves. The average of these is computed and the 16<sup>th</sup>— and 84<sup>th</sup>— percentiles for each frequency are reported to give





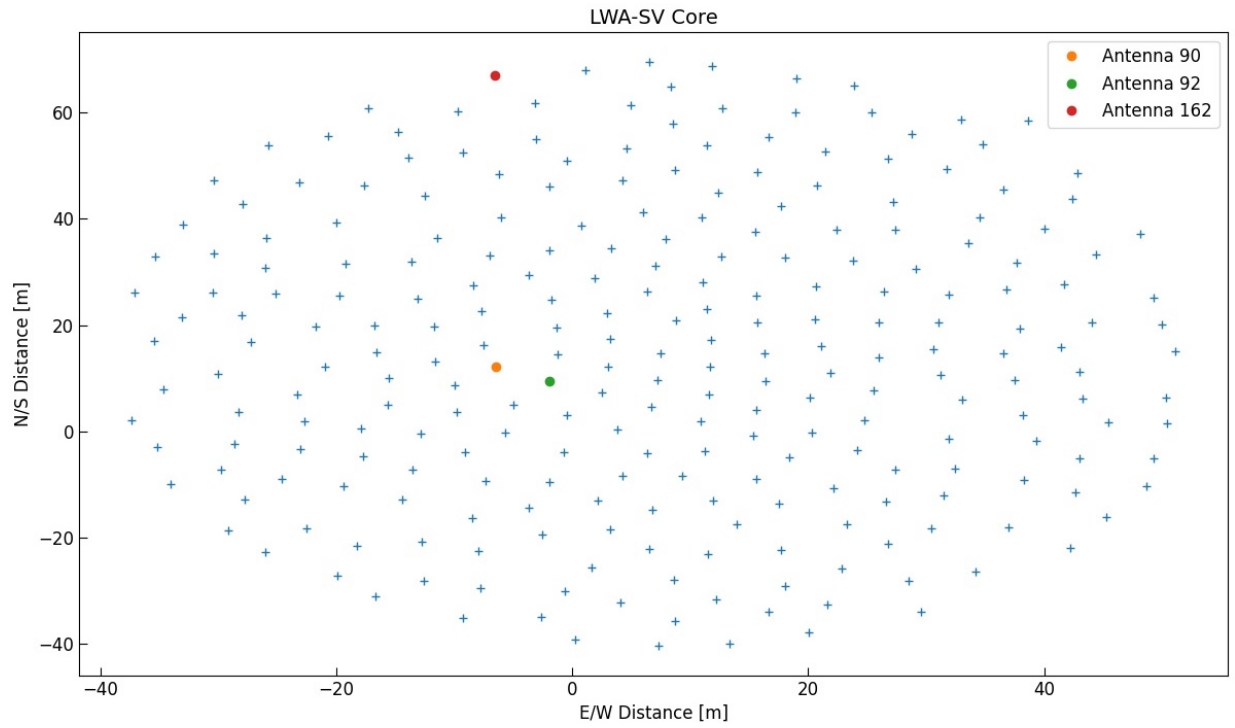
(a) LWA1 Antenna Positions

LWA1 S12 Antenna Coupling Measurements



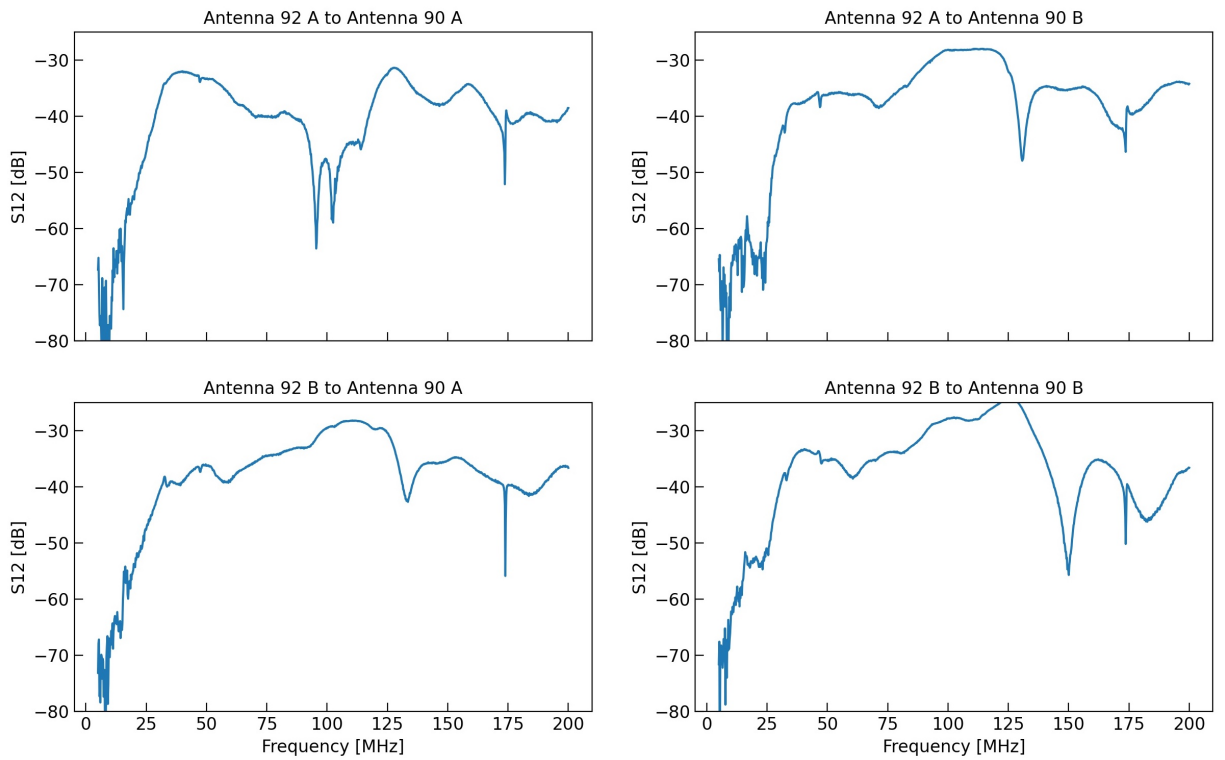
(b) S12 Measurements

**Figure 6.** LWA1 Antenna Mutual Coupling Results. (a) Antenna positions within LWA1 with the measured antennas marked. Antenna 204 is on the North–Eastern edge of the array and was used for the single antenna measurements. Antennas 9 and 10 are embedded in the array and used for antenna mutual coupling measurements. (b) S12 results for the four possible polarization combinations.



(a) LWA-SV Antenna Positions

## LWA-SV S12 Antenna Coupling Measurements



(b) S12 Measurements

**Figure 7.** LWA-SV Antenna Mutual Coupling Results. (a) Antenna positions within LWA-SV with the measured antennas marked. Antenna 162 is on the Northern edge of the array and was used for the single antenna measurements. Antennas 90 and 92 are embedded in the array and used for antenna mutual coupling measurements. (b) S12 results for the four possible polarization combinations.

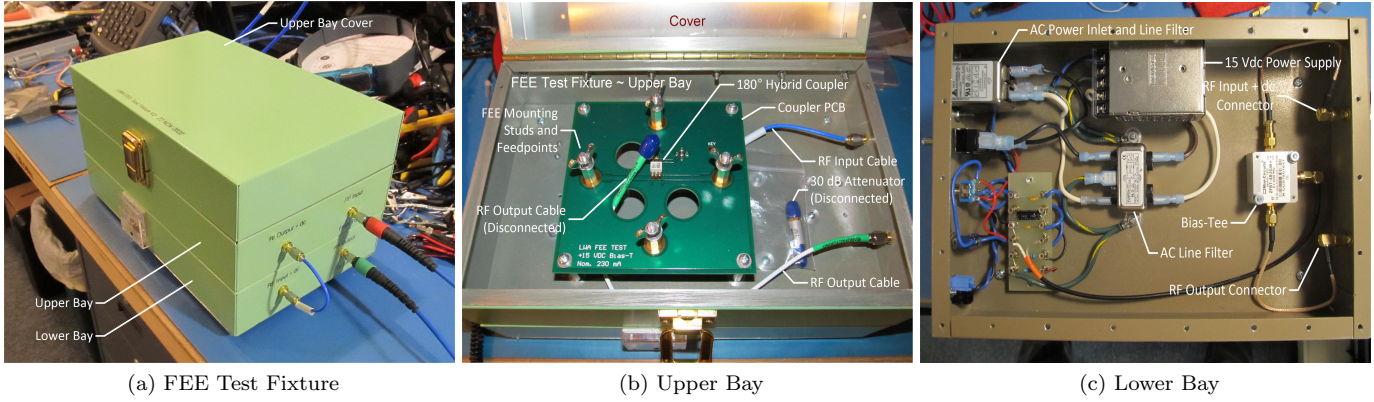


**Figure 8.** FEE Test Fixture box which was fabricated to measure the scattering parameters of the LWA FEE board. It consists of two bays with the upper bay containing a Coupler PCB which converts the unbalanced signal from the VNA to a balanced signal which can be injected into the FEE feedpoints. The lower bay contains a 15 Vdc power supply which powers the FEE-under-test through a bias tee.

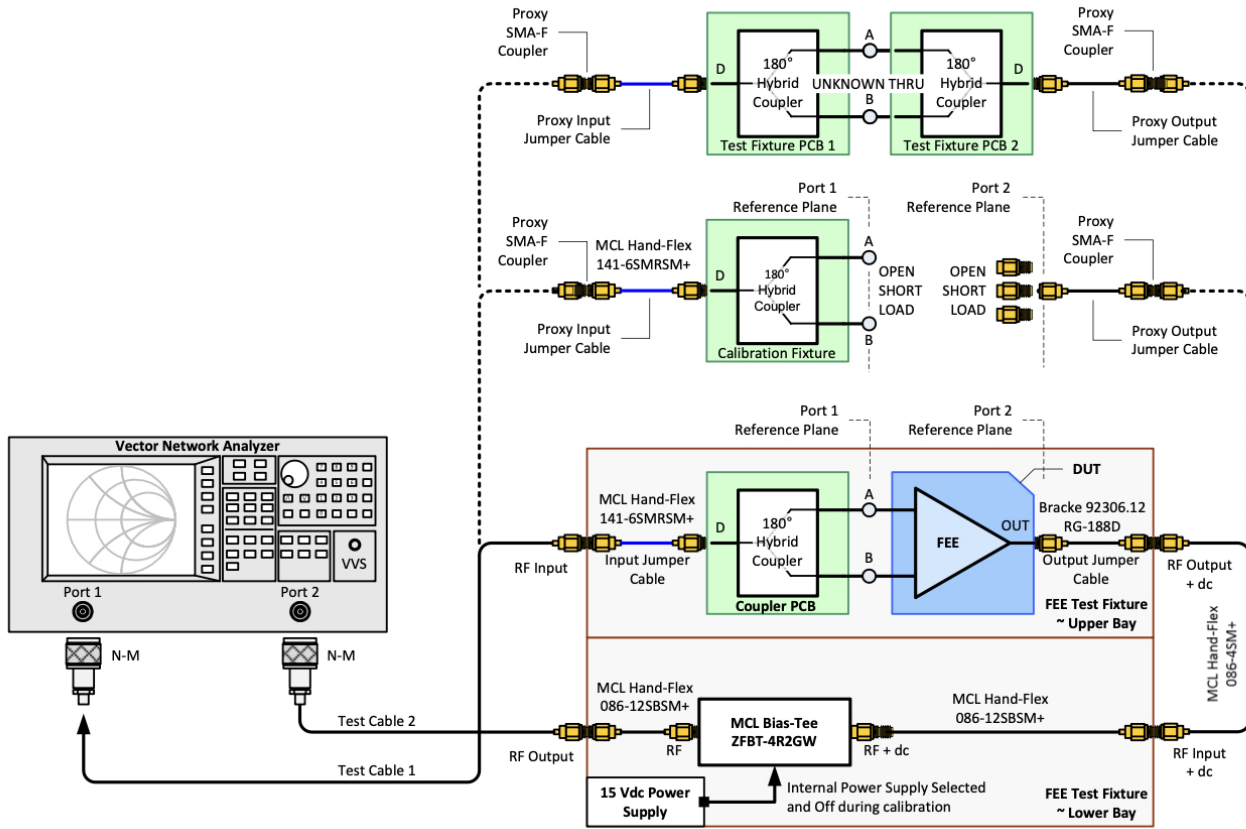


**Figure 9.** LWA FEE Test Fixture box. The FEE Test Fixture box consists of two bays where the FEE-under-test is mounted in the upper bay and a bias tee is located in the lower bay. A  $180^\circ$  hybrid coupler is connected to the VNA in the upper bay in reverse in order to convert the unbalanced signal from the VNA to a balanced signal which can be injected into the FEE. This allows for 2-port scattering parameter measurements of the LWA FEE. The hybrid coupler was de-embedded by using the Calibration Fixtures described in Section 2. This procedure is represented in the plot by the setups depicted with dotted lines. Proxy cables were used to account for the connections internal to the FEE Test Fixture box. The top path shows the Thru calibration, the middle path shows the Short, Open, and Load calibrations, and the bottom path with solid lines show the measurement setup.

$\sim 1\sigma$  uncertainty bounds. The measured scattering parameters of the FEE board and the computed IMF are shown in Figures 10 and 11, respectively.

#### 4. DISCUSSION AND CONCLUSIONS

It is apparent from Figure 11 that the model IME presented in Hicks et al. (2012) generally agrees with the measurements presented in this work. The new measurements imply that the antenna is generally more efficient than previous simulations suggested. In order to get a sense about how much better the new IMF captures impedance mismatch effects in the array, we use it to correct LWA1 Low Frequency Sky Survey and compare to results using the older IME correction. We also included the updated FEE forward gain correction, which is equivalent to S21 shown in Figure 10.

We used data captured using LWA1 on January 20<sup>th</sup>, 2019 and corrected the data for impedance mismatch effects, FEE gain, and analog receiver board (ARX) gain. These are the three primary corrections used in Dowell et al. (2017). In order to gauge whether the corrections improve the quality of the measured sky spectrum, we simulate the LWA dipole beam pattern and convolve it with a realization of the Global Sky Model (GSM, de Oliveira-Costa et al. 2008) at the relevant local sidereal times in order to create a simulated spectrum of the sky. The scales of the raw and simulated spectra must be matched since the observed raw spectrum is in an arbitrary power scale and the simulated spectrum is in units of temperature. The ratio of the median of simulated temperature spectrum to that of raw data spectrum is used as a scaling factor to convert the raw data to temperature. A simple power law of the form

$$T = k \cdot \nu^\alpha, \quad (3)$$

is then fitted to the spectrum and the spectral index,  $\alpha$ , is reported as a first order comparison to the GSM spectrum. It should be noted that this method of assessing the quality of the corrected spectrum is not without caveats. First, there is debate over how accurate the GSM is at low frequencies since it relies on a principle component analysis which uses various input sky maps, most of which do not include frequencies below 100 MHz. Second, there is some uncertainty in how accurate the models of the LWA dipole beam pattern are. Together, the uncertainties in both the GSM and the LWA dipole beam pattern will be present in the simulated spectrum which we take to be the benchmark with which to measure how good our corrections are. This is not desirable, but there are no better alternatives at the present time.

The results of using both the old and new corrections are shown in Figure 12. The biggest difference is the removal of the severe bend in the spectrum which is present in the corrected spectrum that uses the older corrections at frequencies  $\nu \lesssim 45$  MHz. This feature is not expected to be physical in the sky spectrum since the sky at these frequencies is known to be well modeled by a simple power law. Therefore, it is thought to be due to errors in the instrumental correction terms. It is encouraging to see the new correction terms reduce this feature in the corrected spectra.

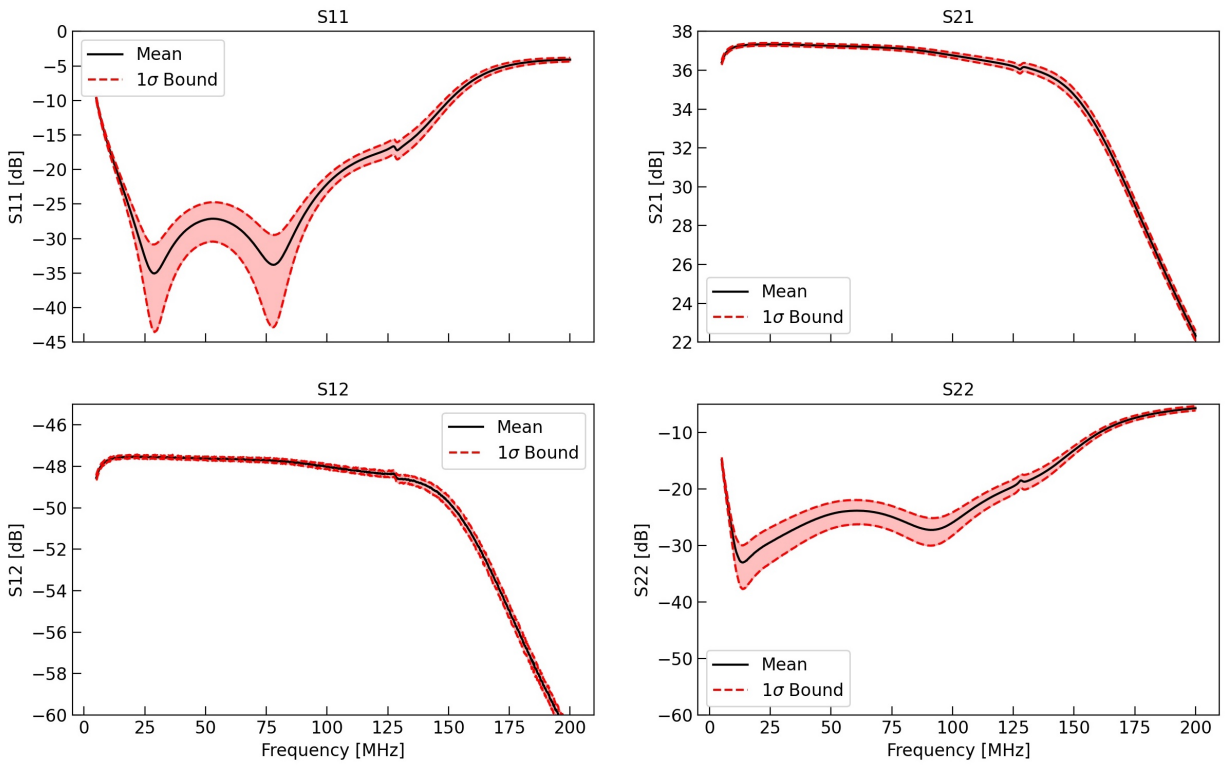
The analysis presented here shows that the new IMF and FEE forward gain corrections result in a measured sky spectrum which is more consistent with physical expectations. However, the spectral index of the power law fit is still off from the expected value of the sky at these frequencies, which is  $\alpha \approx -2.5$ . After updating the impedance mismatch and FEE forward gain corrections, we conclude that the final correction term, the ARX gain term, should be remeasured in follow up work. The current ARX correction is from old measurements carried out in the lab which we are confident can be redone with higher accuracy and a more sophisticated methodology. Obtaining new measurements of the ARX boards is left as future work. The above three corrections do not account for the contribution from the receiver temperature, which is additive in nature and is expected to be frequency dependent. This must also be accounted for in order to fully calibrate the measured spectrum; however, this is beyond the scope of the presented work.

#### 5. SUMMARY

We have carried out 2-port scattering parameter measurements of the LWA antenna and front end electronics (FEE) which can be used to derive correction terms to calibrate LWA data. This had not been done in the past since the reference plane of the VNA must be shifted to the feedpoints where the FEE boards mount to the antenna and the presence of a 180° hybrid coupler on the FEE board prevented this. We developed custom Calibration and Test Fixtures which de-embed the hybrid coupler and shift the VNA reference plane to the antenna feedpoints.

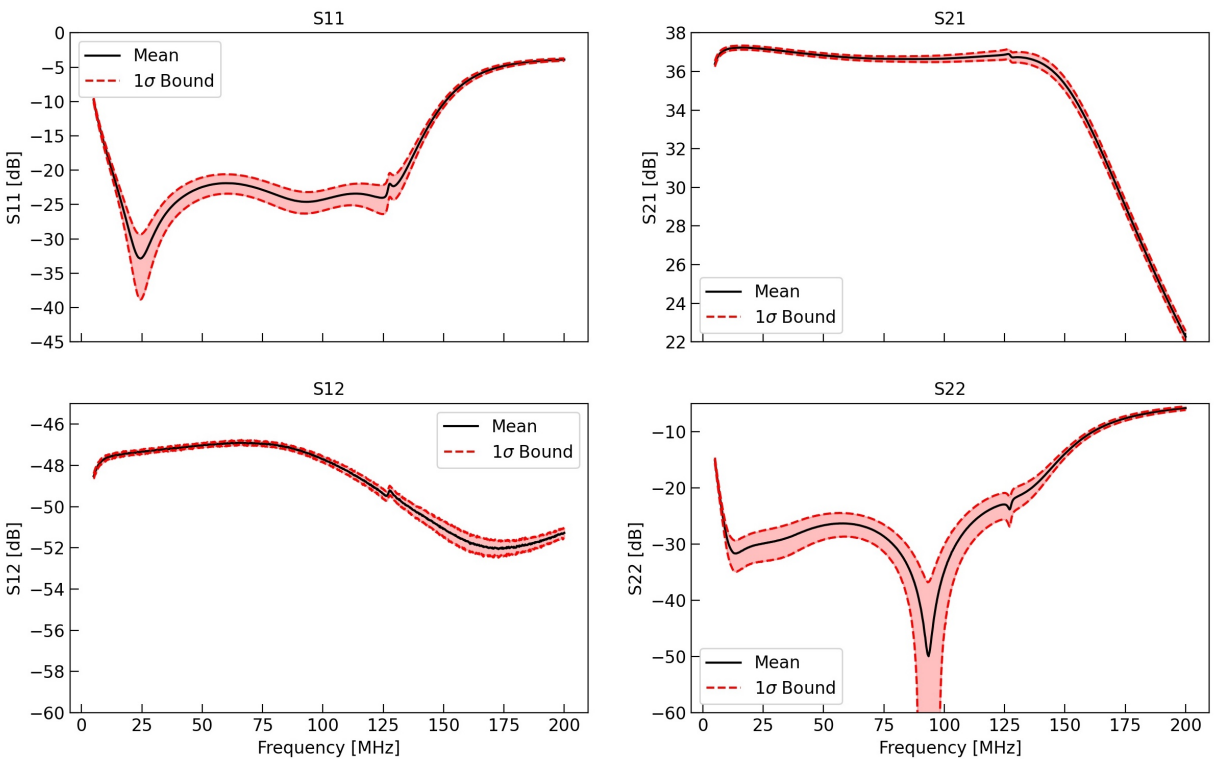
We measured multiple antennas at both commissioned LWA stations in New Mexico, LWA1 and LWA-SV, as well as an isolated antenna located at the site of the future LWA mini-station which will be located at the end of the

LWA FEE S-Parameters (N=10)



(a) Polarization A

LWA FEE S-Parameters (N=10)



(b) Polarization B

**Figure 10.** Scattering parameters of the version 1.8 LWA FEE board. Ten FEE boards were tested and the mean (black line) with  $1\sigma$  bounds (red shaded area) are shown.

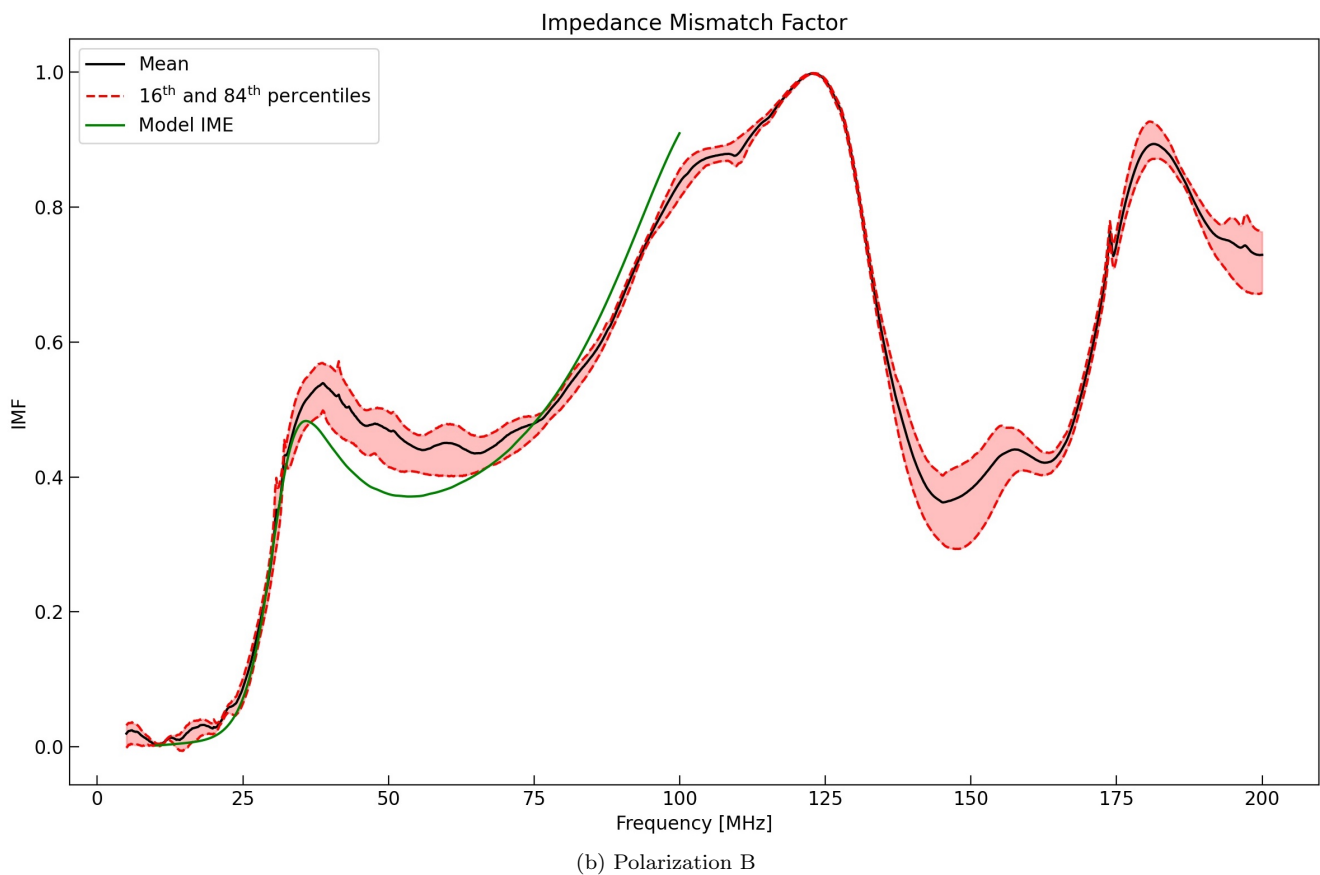
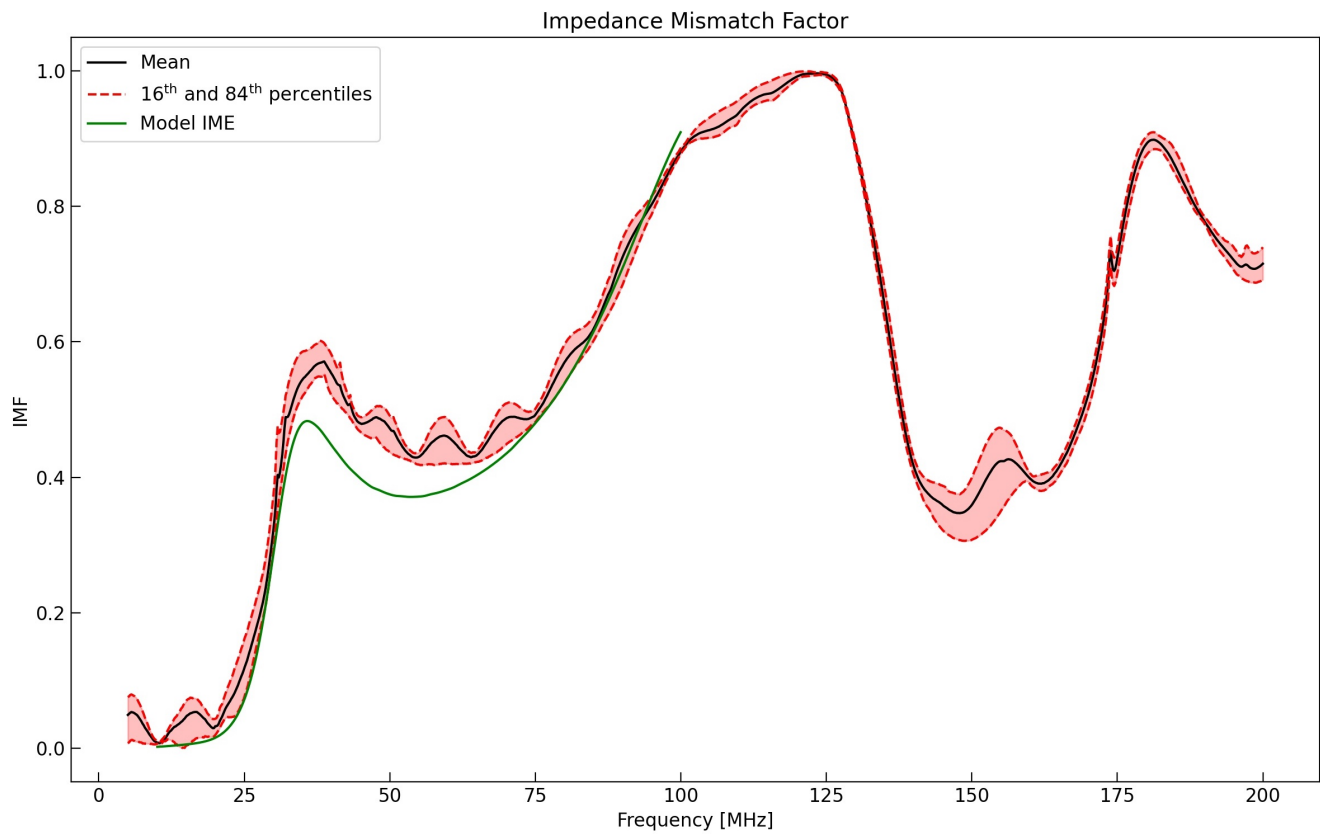


**Figure 11.** Impedance mismatch factor. The black curve is an average over IMF's calculated using different FEE and antenna data. The red shaded area shows the  $\sim 1\sigma$  uncertainty bound. The model IME derived in Hicks et al. (2012) is shown in green.

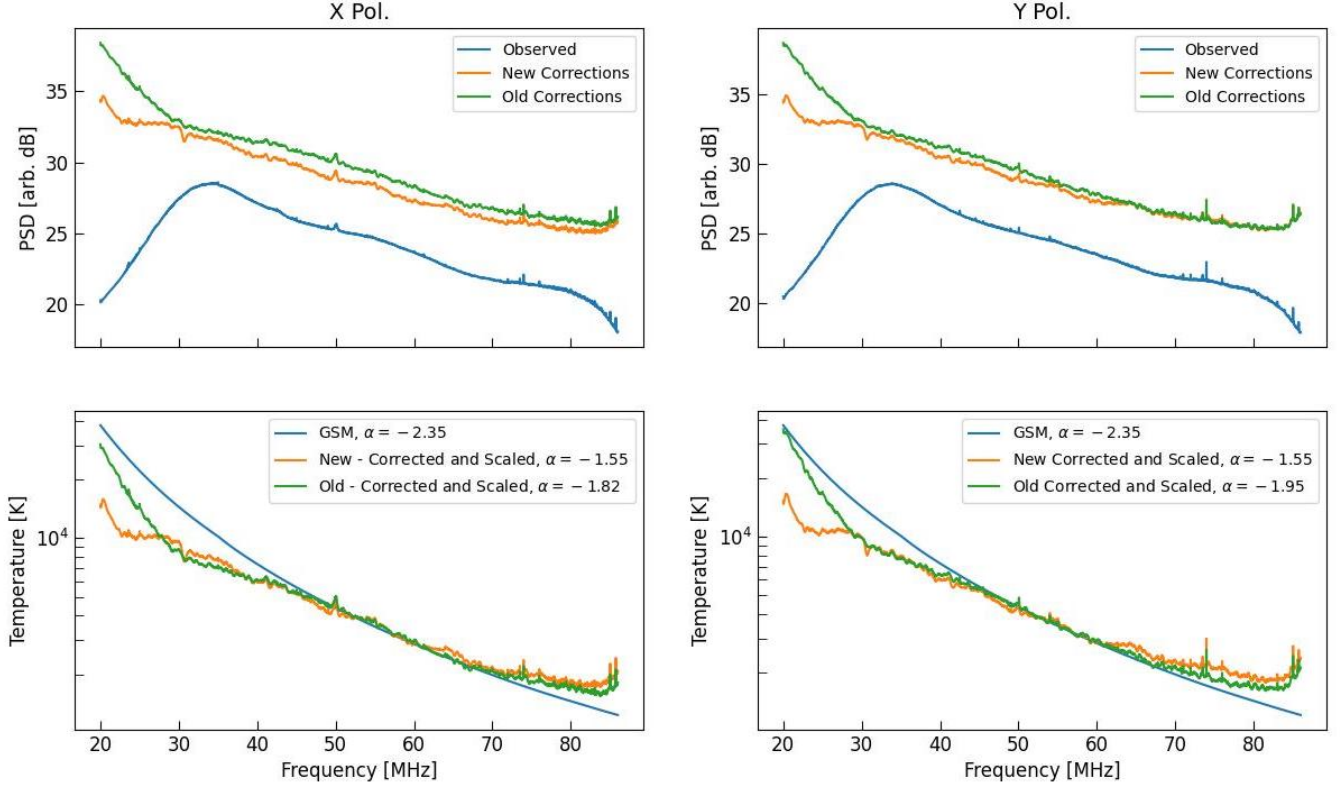


**Figure 12.** Comparison between old and new corrections to the LWA1 Low Frequency Sky Survey. The top panels show the raw observed spectra and corrected spectra. The new corrections include the new IMF measurements and new FEE forward gain measurements presented in this work combined with older measurements of the analog receiver (ARX) gain. The older corrections use the original IME simulations from [Hicks et al. \(2012\)](#) and previous lab-based measurements of the FEE forward gain. The bottom panels show a realization of the GSM convolved with a model of the LWA dipole beam pattern along with the corrected spectra from the top panels after they have been scaled to the median temperature of the GSM spectrum. A simple power law is fit for each spectrum and the best fit spectral index for each is reported in the legend. X polarization corresponds to the dipole arms which are oriented North–South and is denoted Polarization A in other sections of this work. Y polarization similarly corresponds to the East–West dipole arms and is denoted Polarization B in other sections of this work.

North arm of the Very Large Array, LWA–NA. We carried out both single antenna measurements which measure the four associated scattering parameters as well as antenna–antenna coupling measurements which measure the strength of mutual coupling between adjacent elements in the array. Mutual coupling is very difficult to quantify in an array with a large number of elements like the LWA, which makes these the first measurements to ever try to quantify the amount of mutual coupling in a LWA station.

We also measured the scattering parameters for a small sample of FEE boards in order to get updated measurements on the FEE reflection coefficient and forward gain. The FEE reflection coefficient measurements, combined with the single antenna reflection coefficient measurements, yielded an updated impedance mismatch factor (IMF) correction used to remove impedance mismatch effects from LWA data. We verified both the new IMF and FEE forward gain corrections by comparing their effects on LWA1 data captured in January of 2019. We found that the new corrections resulted in the removal of a non-physical feature in the measured sky spectrum which implies that they better represent the physical system than previous simulations. We conclude that we also need to make improved measurements of the analog receiver board (ARX) gain to fully capture instrumental effects for future sky surveys with the LWA.

Christopher DiLullo's research was supported by an appointment to the NASA Postdoctoral Program at NASA Goddard Space Flight Center, administered by Oak Ridge Associated Universities under contract with NASA.

Construction of the LWA has been supported by the Office of Naval Research under Contract N00014-07-C-0147 and by the AFOSR. Support for operations and continuing development of the LWA1 is provided by the Air Force Research Laboratory and the National Science Foundation under grants AST-1835400 and AGS- 1708855.

#### REFERENCES

- Cranmer, M. D., Barsdell, B. R., Price, D. C., et al. 2017, *Journal of Astronomical Instrumentation*, 6, 1750007
- de Oliveira-Costa, A., Tegmark, M., Gaensler, B., et al. 2008, *Monthly Notices of the Royal Astronomical Society*, 388, 247
- DiLullo, C., Dowell, J., & Taylor, G. B. 2021, *Journal of Astronomical Instrumentation*, 10, 2150015
- DiLullo, C., Taylor, G. B., & Dowell, J. 2020, *Journal of Astronomical Instrumentation*, 9, 2050008
- Dowell, J., Taylor, G. B., Schinzel, F. K., Kassim, N. E., & Stovall, K. 2017, *Monthly Notices of the Royal Astronomical Society*, 469, 4537
- Ellingson, S. W. 2011, *IEEE Transactions on Antennas and Propagation*, 59, 1855
- Hicks, B. C., Paravastu-Dalal, N., Stewart, K. P., et al. 2012, *Publications of the Astronomical Society of the Pacific*, 124, 1090
- Rudge, A. W., Milne, K., & Olver, A. D. 1986, *The Handbook of Antenna Design* (P. Peregrinus)
- Taylor, G., Ellingson, S., Kassim, N., et al. 2012, *Journal of Astronomical Instrumentation*, 1, 1250004